Stem Cell Reports
Report
OPEN ACCESS

Craniometaphyseal Dysplasia Mutations in ANKH Negatively Affect Human Induced Pluripotent Stem Cell Differentiation into Osteoclasts

I-Ping Chen,[1,*] Raj Luxmi,[1] Jitendra Kanaujiya,[2] Zhifang Hao,[3] and Ernst J. Reichenberger[2]
[1]Department of Oral Health and Diagnostic Sciences, School of Dental Medicine, University of Connecticut Health, 263 Farmington Avenue, Farmington, CT 06030, USA
[2]Center for Regenerative Medicine and Skeletal Development, Department of Reconstructive Sciences, University of Connecticut Health, Farmington, CT 06030, USA
[3]Department of Cell Biology, Center for Vascular Biology, University of Connecticut Health, Farmington, CT 06030, USA
*Correspondence: ipchen@uchc.edu
https://doi.org/10.1016/j.stemcr.2017.09.016

SUMMARY

We identified osteoclast defects in craniometaphyseal dysplasia (CMD) using an easy-to-use protocol for differentiating osteoclasts from human induced pluripotent stem cells (hiPSCs). CMD is a rare genetic bone disorder, characterized by life-long progressive thickening of craniofacial bones and abnormal shape of long bones. hiPSCs from CMD patients with an in-frame deletion of Phe377 or Ser375 in ANKH are more refractory to *in vitro* osteoclast differentiation than control hiPSCs. To exclude differentiation effects due to genetic variability, we generated isogenic hiPSCs, which have identical genetic background except for the ANKH mutation. Isogenic hiPSCs with ANKH mutations formed fewer osteoclasts, resorbed less bone, expressed lower levels of osteoclast marker genes, and showed decreased protein levels of ANKH and vacuolar proton pump v-ATP6v0d2. This proof-of-concept study demonstrates that efficient and reproducible differentiation of isogenic hiPSCs into osteoclasts is possible and a promising tool for investigating mechanisms of CMD or other osteoclast-related disorders.

INTRODUCTION

Many rare genetic bone disorders result in life-long debilitating symptoms with little or no cures available. Diseases with abnormal bone homeostasis can result from dysfunctional osteoblasts, osteoclasts, or a disrupted interaction between osteoblasts and osteoclasts. Pathogenic mechanisms of rare genetic bone disorders are largely unknown, in part due to the inaccessibility of human skeletal samples and lack of animal models. Studying rare bone diseases can help to better understand normal physiological processes in bone homeostasis and complex disease patterns in common bone disorders such as osteoporosis.

Various somatic cell types have been reprogrammed into hiPSCs, which are capable of indefinite self-renewal and which theoretically can be differentiated into any cell type. While *in vitro* and *in vivo* methods for differentiating hiPSCs into osteoblasts are more advanced (Kang et al., 2016; Kanke et al., 2014; Kuhn et al., 2014; Ochiai-Shino et al., 2014), there are very few publications addressing differentiation into osteoclasts (Choi et al., 2009; Grigoriadis et al., 2010). Current hiPSC-osteoclast differentiation protocols require co-culture systems or numerous cytokines for extended periods of time (Choi et al., 2009; Grigoriadis et al., 2010). The application of hiPSC-based approaches in osteoclast-related disorders has been limited due to difficulties in differentiating hiPSCs into osteoclasts.

Here, we present a simple and reproducible method for differentiating hiPSCs into osteoclasts and apply this tool to examine osteoclast defects in craniometaphyseal dysplasia (CMD) where impaired osteoclastogenesis is a major contributor as shown in a mouse model expressing a Phe377del mutation in the progressive ankyloses gene *Ank* (Chen et al., 2011). CMD is characterized by progressive thickening of craniofacial bones, which can lead to blindness, deafness, facial palsy, severe headaches, and abnormal shape of long bones. Treatment of CMD is limited to risky surgeries to decompress obstructed foramina to relieve symptoms. Mutations for the autosomal dominant form of CMD have been identified in the *ANKH* gene and are mostly one amino acid deletions or insertions that cluster in the C terminus (Nurnberg et al., 2001; Reichenberger et al., 2001). We have used Sendai virus vectors encoding *OCT3/4*, *SOX2*, *KLF4*, *c-MYC* to generate hiPSCs from peripheral blood of healthy donors and CMD patients (Chen et al., 2013). The resulting integration-free hiPSCs are pluripotent, have normal karyotype, are capable of differentiating into cells of the three-germ layers *in vivo* and *in vitro* and are negative for transgene expression after an average of 10–13 passages (Chen et al., 2013). Here, we show that isogenic hiPSCs with CMD-causing ANKH mutation are more refractory to osteoclast formation *in vitro* and propose that the isogenic hiPSC approach has great potential for modeling genetic bone diseases with osteoclast defects.

Table 1. hiPSC Lines with or without CMD Mutations in ANKH			
Sample #	**ANKH Mutation**	**Age**	**Gender**
CMD1	Phe377del (exon 9)	10	male
CMD2	Ser375del (exon 9)	10	female
CMD3	Phe377del (exon 9)	45	female
Isogenic CMD hiPSCs	Phe377del (exon 9)	33	female
Control1	none	30	female
Control2 (clone 2)	none	33	female
Control2 (clone 11)	none	33	female
Isogenic control hiPSCs	none	10	female

RESULTS

Differentiation of hiPSCs into Mature and Functional Osteoclasts

hiPSC lines used in this study were summarized in Table 1. We first used hiPSCs from healthy control individuals to optimize the osteoclast differentiation protocol by direct differentiation through embryoid bodies (EBs). This three-stage protocol consists of EB mesoderm differentiation, expansion of myelomonocytic cells, and maturation of hiPSC osteoclasts (Figure 1A).

EB size can affect the differentiation efficiency of stem cells (Moon et al., 2014; Ng et al., 2005). In order to achieve better consistency in differentiation efficiency, we generated relatively uniformly sized EBs by culturing Accutase-dissociated hiPSCs on Nunclon Sphera microplates, resulting in an average of 150–250 EBs from two wells of 80% confluent hiPSCs on six-well plates (Figure 1B; see also Figures S1A and S1B). We next determined that culturing EBs in Stempro-34 medium supplemented with hBMP4 and hVEGF for 2 days followed by hBMP4, hVEGF, hSCF, hTPO, hFLT3, and hbFGF for another 2 days is most efficient for inducing the expression of mesoderm marker genes (see also Figures S1C and S1D; Table S1). Levels of *HAND1* (*Heart and neural crest derivatives expressed 1*), *SCL* (*TAL-1, Stem cell leukemia*), *T* (*brachyury*), *CDX2* (*Caudal type homeobox 2*), and *CD34* mRNA were significantly increased in EBs cultured for 4 days, suggesting efficient mesoderm differentiation (Figure 1B).

For stage 2, EBs were transferred to gelatin-coated plates and cultured with hM-CSF and hIL-3. We collected floating monocytes released from adherent EBs after 10, 13, 17, and 21 days for fluorescence-activated cell sorting analysis. The expansion of myelomonocytic populations was assessed by expression analysis of CD14, CD43, and CD45. At day 17, CD14, CD43, and CD45 levels of hiPSC monocytes consistently expressed highest with less variability than at day 13 and dropped at day 21 (Figure 1C; see also Figure S2). Cells collected at day 17 of stage 2 culture were processed into stage 3 by supplementing with vitamin D, hTGFβ, hM-CSF, and hRANKL to generate mature osteoclasts, which stained positive for TRAP, resorbed bone chips, and expressed osteoclast marker genes *TRAP* (*Tartrate-resistant acid phosphatase type 5; APC5*) and *CATHEPSIN K* (*CTSK*) (Figure 1D).

CMD hiPSCs Are More Refractory to Osteoclast Differentiation *In Vitro*

We next applied our osteoclast differentiation protocol to hiPSCs from three CMD patients (CMD1, CMD2, CMD3). Analysis of osteoclastogenesis progression was performed at day 10 of stage 3. CMD1 and CMD2 hiPSCs formed less TRAP+ multinucleated cells (nuclei ≥ 3), whereas the number of osteoclasts from CMD3 was statistically insignificant from healthy controls (Figure 2A). Smaller-sized osteoclasts is a characteristic feature observed in a CMD mouse model and in peripheral blood cultures of CMD patients (Chen et al., 2009, 2011). Consistently, hiPSC-derived osteoclasts from patients CMD1 and CMD2 were also reduced in size (Figure 2B). CMD hiPSCs (combined data from CMD1, 2, and 3) showed significantly reduced expression of osteoclast marker genes *TRAP*, *CTSK*, and *CALCITONIN RECEPTOR*, while *NFATc1* (*Nuclear factor of activated T-cells 1*) did not significantly differ between control and CMD patient samples (Figure 2C). All osteoclast markers significantly increased in mature osteoclasts compared with undifferentiated osteoclasts from healthy donors and CMD patients (Figure 2C). We noticed a large variability in osteoclast numbers and marker gene expression within CMD patients (see also Figure S3). These differences may result from the variability in age, sex, or genetic background. To minimize these variations, we decided to generate isogenic hiPSCs and performed further analyses, including bone resorption assays, in these cells.

CMD Mutations in *ANKH* Diminish Isogenic hiPSC Differentiation into Osteoclasts

Isogenic hiPSCs have identical genetic background except for a disease mutation (genetic variant), allowing researchers to determine the impact of a specific mutation (Cong et al., 2013; Ran et al., 2013; Yoshimi et al., 2016). We introduced the *ANKH* Phe377del (F377del) mutation into healthy hiPSCs (healthy donor 2) and corrected a Ser375del *ANKH* mutation from a CMD patient (CMD2) by CRISPR/Cas9 technology. Inserted mutation or correction of *ANKH* was confirmed by sequencing (Figure 3A).

For this proof-of-concept study, we used two pairs of isogenic hiPSCs, hiPSCs with or without a homozygous F377del and hiPSCs with or without a heterozygous S375del mutation in ANKH. We expected that both

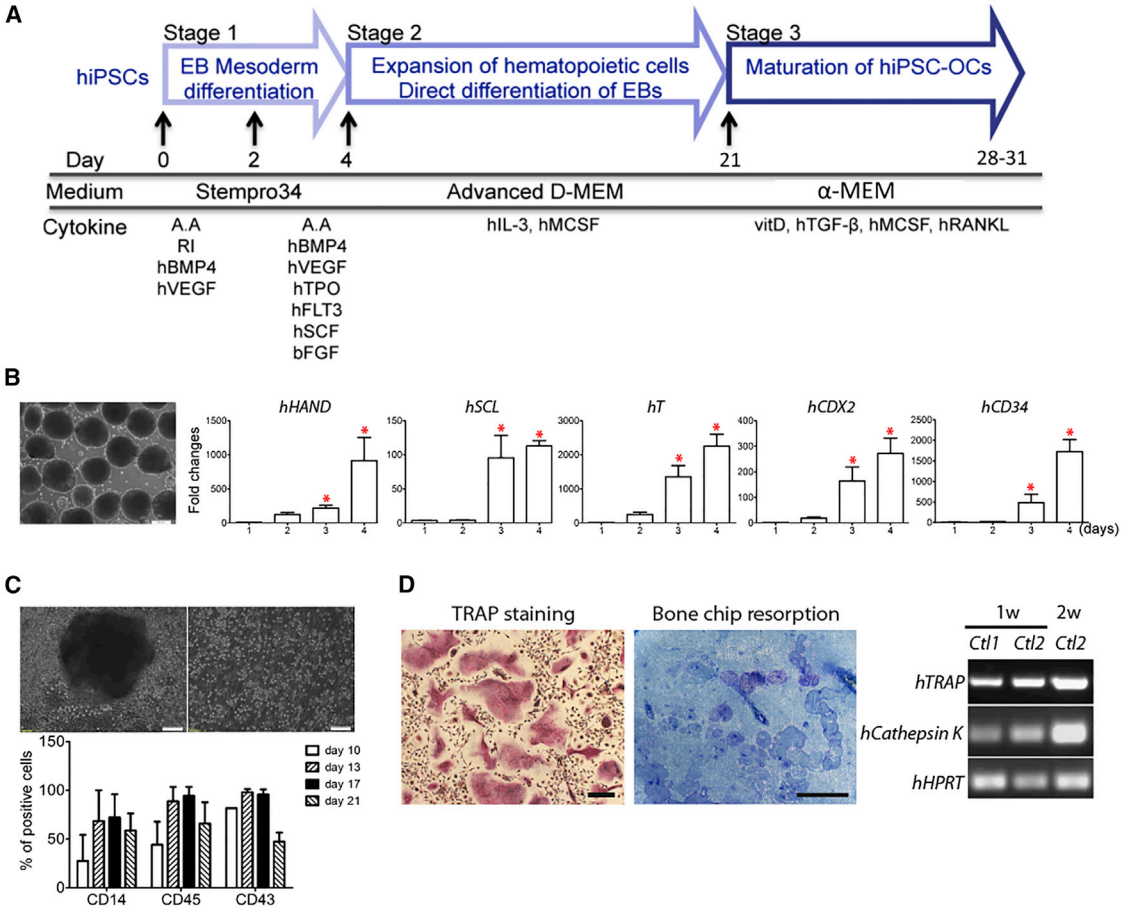

Figure 1. Differentiating Healthy Control hiPSCs into Osteoclasts

(A) Schematic protocol of differentiating hiPSCs into osteoclasts.

(B) Embryoid body (EB) formation and mesoderm gene expression. EBs cultured for 4 days (left panel). Scale bar, 200 μm. Expression of mesoderm marker genes in EBs cultured for 1, 2, 3, and 4 days by qPCR. *p < 0.05 by one-way ANOVA. Data presented are means ± SD.

(C) Myelomonocytic cell expansion. Single cells released from EBs into suspension (top panel). Scale bar, 100 μm. Percentage of cells positive for hematopoietic cell surface markers CD14, CD43, and CD45 in cells released from 10, 13, 17, and 21 day adherent EBs by flow cytometry. Data presented are means ± SD.

(D) TRAP+ osteoclasts differentiated from hiPSCs (left panel), resorption pits on bone chips (middle panel), and expression of OC marker genes, *TRAP* and *CTSK* by RT-PCR (right panel). *HPRT* served as internal control. Ctl1, control1; Ctl2, control2; 1w, 2w, 1 or 2 weeks in stage 3. Scale bar, 100 μm (left panel) and 200 μm (middle panel). Three independent experiments (three technical replicates per experiment) for each hiPSC line. Data were pooled from four wild-type hiPSC lines (hiPSCs from two healthy subjects, two hiPSC clones of each individual donor).

ANKH mutations have similar effects on osteoclastogenesis and the effects of ANKH mutations are dose dependent. While differentiating into osteoclasts, the CMD mutant isogenic hiPSCs formed significantly less osteoclasts and resorbed less on bone chips than those expressing wild-type ANKH (Figures 3B and 3C). As expected, hiPSCs with the homozygous CMD mutation (F377del) showed the least osteoclast numbers (Figure 3B). Osteoclasts differentiated from isogenic hiPSCs with ANKH mutations had reduced numbers of nuclei, which is an indication of a fusion defect (Figure 3D). *TRAP*, *CTSK*, *CALCR*, and *NFATc1* were significantly reduced in isogenic hiPSC-derived osteoclasts with a Ser375del mutation (Figure 3E).

A published study showed in a single CMD patient that the osteoclast-reactive vacuolar proton pump was not expressed but was expressed in cells derived from the patient's mother (Yamamoto et al., 1993). Vacuolar proton pump subunit D2 (v-ATPase V_0 domain subunit d2, Atp6v0d2) is expressed in osteoclasts, not in osteoblasts, and plays an important role in osteoclast fusion (Lee et al., 2006). We first examined the expression of Atp6v0d2 in isogenic hiPSCs by immunoblots. Atp6v0d2 was not expressed in

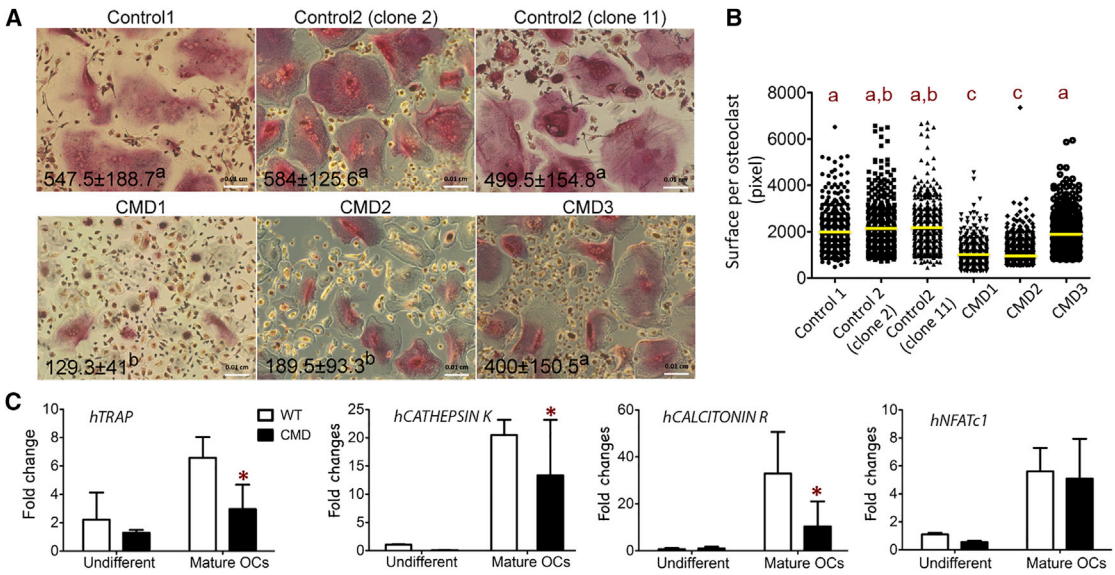

Figure 2. Osteoclasts Differentiated from Healthy Control and CMD hiPSCs

(A) Comparison of control and CMD osteoclasts derived from hiPSCs. Numbers of TRAP+ multinucleated cells (nuclei ≥ 3) are shown (mean ± SD) in the left corners of the images. Different letters (a, b) indicate statistically significant difference ($p < 0.05$) by one-way ANOVA. Scale bar, 100 μm.

(B) Decreased sizes of osteoclasts derived from CMD1 and CMD2 hiPSCs. Yellow bars indicate the mean value of each group ($n \geq 400$ osteoclasts measured per group). Different letters (a, b, c) indicate statistically significant difference ($p < 0.05$) by one-way ANOVA.

(C) Decreased expression of *TRAP*, *CATHEPSIN K*, *CALCITONIN RECEPTOR* mRNA message in osteoclasts differentiated from CMD hiPSCs shown by qPCR. *$p < 0.05$ by two-way ANOVA. Data presented are means ± SD. Three independent experiments (technical replicates) were performed for each hiPSC line.

undifferentiated hiPSCs but was expressed in hiPSC-derived osteoclasts (Figure 3F). hiPSC-derived osteoclasts with ANKH mutations expressed lower levels of Atp6v0d2 compared with wild-type lines (Figure 3F). We next examined the expression of ANKH in hiPSCs during osteoclast differentiation. We had previously shown that *Ank* mRNA levels in wild-type and *Ank* knockin (KI) mice ($Ank^{KI/KI}$) increase comparably in mature osteoclasts (Chen et al., 2011). We observed similar findings in hiPSC-differentiated osteoclasts (data not shown). ANKH protein was almost undetectable in undifferentiated hiPSCs but was significantly increased in osteoclasts differentiated from hiPSCs (Figure 3G). Interestingly, ANKH protein levels were higher in wild-type hiPSC osteoclasts compared with CMD hiPSC osteoclasts (Figure 3G). Reduced ANKH protein expression was also found in osteoblasts from bone explant cultures from a CMD patient compared with a healthy donor (see also Figure S4). These data demonstrate that isogenic hiPSC-derived bone cells can overcome obstacles of studying rare genetic bone disorders because obtaining human specimens such as bone for explant cultures is difficult, while hiPSCs can easily be obtained from peripheral blood of patients. It is yet unknown whether the reduced amount of ANKH protein is due to decreased osteoclast differentiation in CMD hiPSCs, to abnormal protein processing, or to instability of mutant ANKH. However, these data suggest that CMD pathogenesis may be partially due to decreased amounts of functional ANKH.

DISCUSSION

The potential of hiPSCs in disease modeling or treatment is widely recognized, and methods for generating hiPSCs are well established. The main obstacle is consistency in differentiating hiPSCs into specific cell lineages. Published methods for differentiating hiPSCs into osteoclasts use (1) co-culturing hiPSCs with OP9 cells, a newborn calvarial-derived stromal cell line from mice deficient in macrophage colony stimulating factor (M-CSF) or (2) direct differentiation of hiPSC-derived EBs supplemented with multiple cytokines (Choi et al., 2009; Grigoriadis et al., 2010; Jeon et al., 2016). One of the critical steps of the co-culture method is to match proper cell densities of undifferentiated hiPSCs and OP9 cultures simultaneously. OP9 cells are commonly used to stimulate hematopoietic differentiation from embryonic stem cells and can rapidly differentiate into adipocytes especially at high cell density (Nakano et al., 1994; Wolins et al., 2006). To differentiate hiPSCs

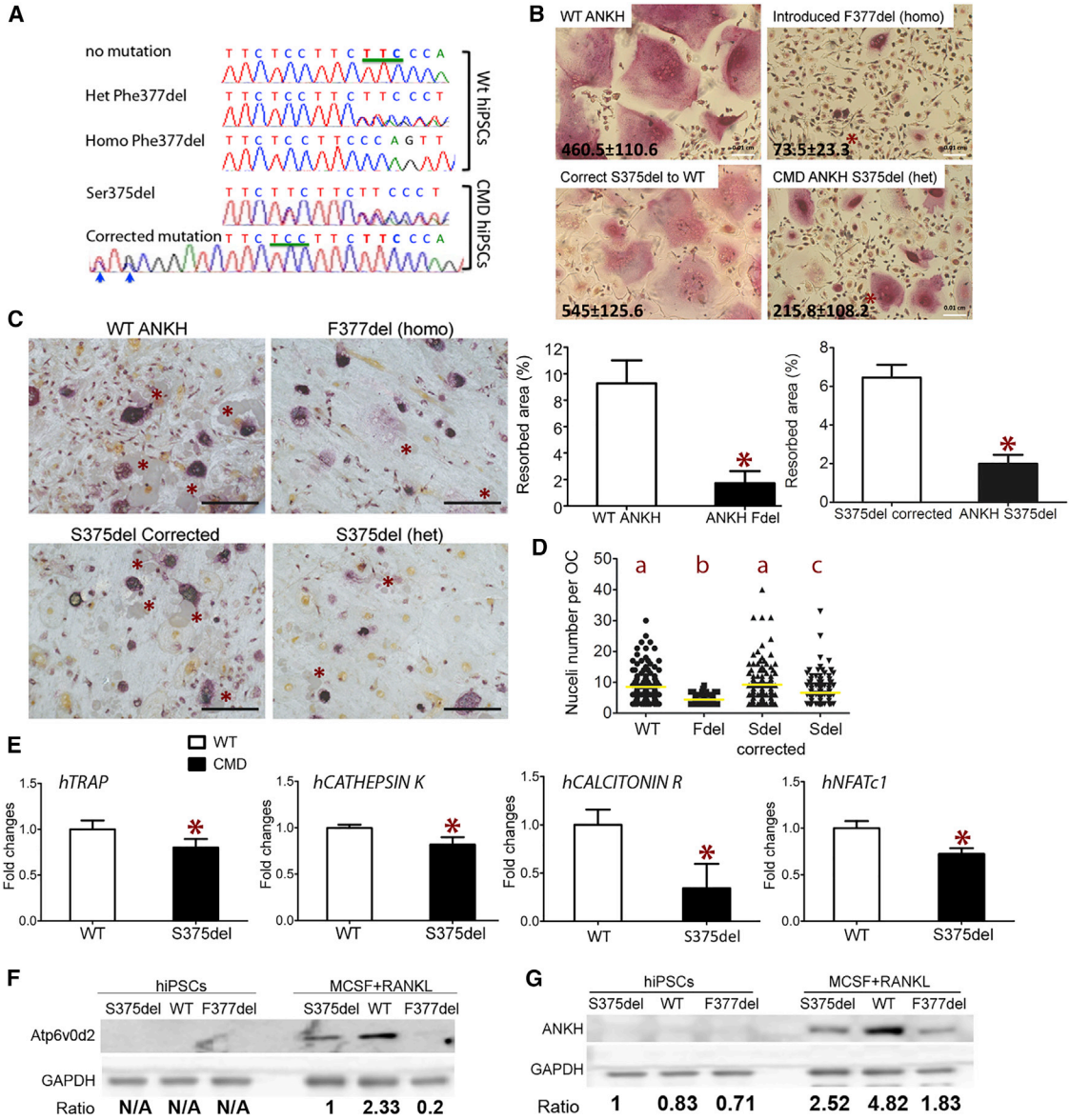

Figure 3. Osteoclasts Differentiated from Isogenic hiPSC with or without CMD *ANKH* Mutations

(A) Electropherograms showing partial sequences of ANKH exon 9 with insertion of Phe377del into wild-type hiPSCs and correction of Ser375del *ANKH* in CMD hiPSCs. Blue arrows indicate silent mutations introduced to minimize recutting of a repaired site.

(B) Decreased numbers of TRAP+ multinucleated osteoclasts formed from isogenic CMD mutant hiPSCs compared with wild-type controls. Numbers of TRAP+ multinucleated cells (nuclei ≥ 3) are shown (mean ± SD) in the left corners of the images. * indicates statistical significance compared with the parental isogenic hiPSCs by Student's t test. Scale bar, 100 μm.

(C) Decreased resorbed area on bone chips by osteoclasts derived from isogenic CMD mutant hiPSCs compared with wild-type controls. * on bone images (left panel) indicate resorption pits. Bar figures show the percentage of resorbed area (mean ± SD). Scale bar, 200 μm. * indicates statistical significance compared with the parental isogenic hiPSCs by Student's t test.

(D) Decreased nuclei numbers in CMD hiPSC-derived osteoclasts (n = 70–156 cells per group). Yellow bar indicates the mean value of each group. Different letters (a, b, c) indicate statistically significant difference ($p < 0.05$) by one-way ANOVA followed by Bonferroni post hoc test.

(E) Decreased expression of *TRAP*, *CATHEPSIN K*, *CALCITONIN RECEPTOR*, *NFATc1* in osteoclasts differentiated from isogenic hiPSCs with a S375del mutation in *ANKH* by qPCR. *$p < 0.05$ by Student's t test. Data presented are means ± SD.

(F) A representative Atp6v0d2 (40 kDa) immunoblot of hiPSCs (left panel) and hiPSC-differentiated osteoclasts (right panel) with or without S375del or F377del ANKH mutations. GAPDH served as loading control. Samples with wild-type and a S375del mutation in ANKH

(legend continued on next page)

into osteoclasts, multiple cytokines are required. While 6–7 cytokines were used by Grigoriadis et al. (2010) for a minimum of 14 days to promote hematopoietic specification and myeloid expansion, we reduced medium supplementation with these many cytokines to 2 days during mesoderm differentiation. We then adapted a published protocol using M-CSF and IL-3 for myeloid differentiation (Jeon et al., 2016; Panicker et al., 2012). The advantages of our method include the following: (1) no need for co-cultures; (2) generation of uniformly sized EBs to minimize variations in differentiation efficiency; (3) rapid expansion of $CD14^+$, $CD43^+$, and $CD45^+$ populations; (4) less cytokines used; and (5) sufficient numbers of osteoclasts for subsequent molecular analyses.

We used Rock inhibitor (Y-27632) to improve survival of Accutase-dissociated hiPSCs as shown previously (Watanabe et al., 2007). Efficient mesoderm differentiation is achieved by effects of several cytokines. BMP4 induces primitive streak and early hematopoietic gene expression and, together with VEGF, can increase expression of *SCL* and *CD34* (Pick et al., 2007). SCF promotes *in vitro* proliferation of primitive hematopoietic progenitors (Hoffman et al., 1993). Together SCF, FLT-3, and TPO play several important roles in human hematopoiesis (Bhatia et al., 1997; Zandstra et al., 1998). bFGF stimulates cell proliferation during hematopoietic differentiation (Pick et al., 2007).

The murine $CD11b^{-/low}B220^-CD3^-CD115^{high}CD^{117+}$ population in bone marrow has the highest osteoclastogenic activity (Jacquin et al., 2006), but human osteoclast precursors are less defined. Choi et al. (2009) enriched myeloid progenitors by expanding hiPSC-derived $Lin^-CD34^+CD43^+CD45^+$ cells and Grigoriadis et al. (2010) used $CD45^+$ as a progenitor marker. We evaluated the myelomonocytic cell expansion by CD14, CD43, and CD45. Although $CD43^+$ and $CD45^+$ are highly expanded, the $CD14^+$ population appears to be variable between samples. $CD14^+$ cells have been shown to form mature and functional osteoclasts and $CD14^-$ cells express osteoclastogenic factors to support $CD14^+$ cells (Costa-Rodrigues et al., 2011; Taylor et al., 2012). In this study, we did not perform population selection by cell sorting.

The pathogenic mechanisms leading to CMD are complex. To date, the only known function of ANK/ANKH is to transport pyrophosphate (Ho et al., 2000). A KI mouse model ($Ank^{KI/KI}$) expressing the human Phe377del mutation in *Ank* replicates many skeletal features of human CMD (Chen et al., 2009). In $Ank^{KI/KI}$ mice, the extracellular PPi levels were comparable with wild-type mice possibly due to compensatory effects of Enpp1 (Chen et al., 2011). Shared CMD phenotypes between $Ank^{null/null}$ and $Ank^{KI/KI}$ mice and decreased ANKH protein in CMD hiPSC-derived osteoclasts suggest that decreased functional ANKH partially contributes to CMD. However, we believe that it involves more than just loss of function of the pyrophosphate transporting activity of ANKH because *Ank* knockout mice do not fully replicate the CMD phenotype (Chen et al., 2009). In this study, we did not report PPi levels in hiPSC-derived osteoclasts.

Lack of osteoclast-reactive vacuolar proton pump expression was reported in one CMD patient where the ANKH mutation had not been identified (Yamamoto et al., 1993). This patient displayed severe sclerotic diaphyseal bone, which is not typical for most cases of CMD caused by ANKH mutations (Yamamoto et al., 1993). Our data showed significantly reduced expression of Atp6v0d2 in isogenic hiPSC-derived osteoclasts expressing CMD mutant ANKH compared with wild-type cells. Whether decreased Atp6v0d2 is caused by lower levels of ANKH and how decreased numbers of vacuolar proton pumps affect CMD pathogenesis needs to be investigated in a future study.

Osteoclast defects in CMD have been shown in our mouse model and in human peripheral blood cultures (Chen et al., 2011; Yamamoto et al., 1993). This study identifies osteoclast defects in CMD using patient-specific hiPSC cultures. Although human osteoclasts can be derived from peripheral blood, it is not realistic to repeatedly obtain blood or bone marrow samples from patients with rare disorders. Therefore, our protocol for differentiating hiPSCs into osteoclasts with high efficiency and reproducibility enables researchers to generate a sufficient supply of human osteoclasts. This proof-of-concept study shows that osteoclasts differentiated from hiPSCs can provide an unlimited source of cells for modeling genetic bone diseases with osteoclast defects and will allow us to investigate the underlying molecular defect as well as to test potential therapeutics.

EXPERIMENTAL PROCEDURES

The animal protocol (101425-0819) was approved by the Institutional Animal Care and Use Committee (IACUC) of University of Connecticut Health, and all work was performed in an AAALAC

are isogenic hiPSCs. The F377del cell lysate is from patient CMD1 hiPSCs and hiPSC-derived osteoclasts. Numbers below indicate ratio of Atp6v0d2 to GAPDH.

(G) A representative ANKH (52 kDa) immunoblot of undifferentiated hiPSCs (left panel) and hiPSC-derived osteoclasts (right panel) with or without S375del or F377del ANKH mutations. GAPDH served as loading control. Samples with wild-type and a S375del mutation are isogenic hiPSCs. The F377del cell lysate is from patient CMD1 hiPSCs and hiPSC-derived osteoclasts. Numbers below indicate the ratio of ANKH to GAPDH. Three independent experiments (technical replicates) were performed for each isogenic hiPSC line.

accredited facility. All studies involving human protocols were in accordance with guidelines of the Institutional Review Board of the University of Connecticut Health (IRB protocol 09-199). Integration-free hiPSC lines from peripheral blood were generated as previously described (Dutra et al., 2013). Information on age, gender, and ANKH mutations of hiPSC lines are summarized in Table 1. We used two different clones (clone2 and clone11) from control2 hiPSC line. Three independent experiments were performed for each hiPSC line (technical triplicates). Statistical analysis was performed using Prism 5 software (GraphPad Software). A p value of less than 0.05 was considered statistically significant. Additional methods are available in Supplemental Experimental Procedures.

SUPPLEMENTAL INFORMATION

Supplemental Information includes Supplemental Experimental Procedures, four figures, and two tables and can be found with this article online at https://doi.org/10.1016/j.stemcr.2017.09.016.

AUTHOR CONTRIBUTIONS

R.L., Z.H., and J.K. performed molecular analysis. I.-P.C. directed the research, performed experiments, and analyzed data. I.-P.C. and E.J.R. wrote the manuscript. All authors approved the manuscript.

ACKNOWLEDGMENTS

We appreciate help from the Stem Cell core and Flow Cytometry core at UConn Health. This work was supported by NIH/NIDCR R00 (DE021442) to I.-P.C.

Received: March 13, 2017
Revised: September 20, 2017
Accepted: September 22, 2017
Published: October 19, 2017

REFERENCES

Bhatia, M., Bonnet, D., Kapp, U., Wang, J.C., Murdoch, B., and Dick, J.E. (1997). Quantitative analysis reveals expansion of human hematopoietic repopulating cells after short-term ex vivo culture. J. Exp. Med. *186*, 619–624.

Chen, I.P., Fukuda, K., Fusaki, N., Iida, A., Hasegawa, M., Lichtler, A., and Reichenberger, E.J. (2013). Induced pluripotent stem cell reprogramming by integration-free Sendai virus vectors from peripheral blood of patients with craniometaphyseal dysplasia. Cell Reprogram *15*, 503–513.

Chen, I.P., Wang, C.J., Strecker, S., Koczon-Jaremko, B., Boskey, A., and Reichenberger, E.J. (2009). Introduction of a Phe377del mutation in ANK creates a mouse model for craniometaphyseal dysplasia. J. Bone Miner Res. *24*, 1206–1215.

Chen, I.P., Wang, L., Jiang, X., Aguila, H.L., and Reichenberger, E.J. (2011). A Phe377del mutation in ANK leads to impaired osteoblastogenesis and osteoclastogenesis in a mouse model for craniometaphyseal dysplasia (CMD). Hum. Mol. Genet. *20*, 948–961.

Choi, K.D., Vodyanik, M.A., and Slukvin, I.I. (2009). Generation of mature human myelomonocytic cells through expansion and differentiation of pluripotent stem cell-derived lin-CD34+CD43+CD45+ progenitors. J. Clin. Invest. *119*, 2818–2829.

Cong, L., Ran, F.A., Cox, D., Lin, S., Barretto, R., Habib, N., Hsu, P.D., Wu, X., Jiang, W., Marraffini, L.A., et al. (2013). Multiplex genome engineering using CRISPR/Cas systems. Science *339*, 819–823.

Costa-Rodrigues, J., Fernandes, A., and Fernandes, M.H. (2011). Spontaneous and induced osteoclastogenic behaviour of human peripheral blood mononuclear cells and their CD14(+) and CD14(-) cell fractions. Cell Prolif. *44*, 410–419.

Dutra, E.H., Chen, I.P., and Reichenberger, E.J. (2013). Dental abnormalities in a mouse model for craniometaphyseal dysplasia. J. Dent. Res. *92*, 173–179.

Grigoriadis, A.E., Kennedy, M., Bozec, A., Brunton, F., Stenbeck, G., Park, I.H., Wagner, E.F., and Keller, G.M. (2010). Directed differentiation of hematopoietic precursors and functional osteoclasts from human ES and iPS cells. Blood *115*, 2769–2776.

Ho, A.M., Johnson, M.D., and Kingsley, D.M. (2000). Role of the mouse ank gene in control of tissue calcification and arthritis. Science *289*, 265–270.

Hoffman, R., Tong, J., Brandt, J., Traycoff, C., Bruno, E., McGuire, B.W., Gordon, M.S., McNiece, I., and Srour, E.F. (1993). The in vitro and in vivo effects of stem cell factor on human hematopoiesis. Stem Cells *11* (*Suppl 2*), 76–82.

Jacquin, C., Gran, D.E., Lee, S.K., Lorenzo, J.A., and Aguila, H.L. (2006). Identification of multiple osteoclast precursor populations in murine bone marrow. J. Bone Miner Res. *21*, 67–77.

Jeon, O.H., Panicker, L.M., Lu, Q., Chae, J.J., Feldman, R.A., and Elisseeff, J.H. (2016). Human iPSC-derived osteoblasts and osteoclasts together promote bone regeneration in 3D biomaterials. Sci. Rep. *6*, 26761.

Kang, H., Shih, Y.R., Nakasaki, M., Kabra, H., and Varghese, S. (2016). Small molecule-driven direct conversion of human pluripotent stem cells into functional osteoblasts. Sci. Adv. *2*, e1600691.

Kanke, K., Masaki, H., Saito, T., Komiyama, Y., Hojo, H., Nakauchi, H., Lichtler, A.C., Takato, T., Chung, U.I., and Ohba, S. (2014). Stepwise differentiation of pluripotent stem cells into osteoblasts using four small molecules under serum-free and feeder-free conditions. Stem Cell Rep. *2*, 751–760.

Kuhn, L.T., Liu, Y., Boyd, N.L., Dennis, J.E., Jiang, X., Xin, X., Charles, L.F., Wang, L., Aguila, H.L., Rowe, D.W., et al. (2014). Developmental-like bone regeneration by human embryonic stem cell-derived mesenchymal cells. Tissue Eng. Part A. *20*, 365–377.

Lee, S.H., Rho, J., Jeong, D., Sul, J.Y., Kim, T., Kim, N., Kang, J.S., Miyamoto, T., Suda, T., Lee, S.K., et al. (2006). v-ATPase V0 subunit d2-deficient mice exhibit impaired osteoclast fusion and increased bone formation. Nat. Med. *12*, 1403–1409.

Moon, S.H., Ju, J., Park, S.J., Bae, D., Chung, H.M., and Lee, S.H. (2014). Optimizing human embryonic stem cells differentiation efficiency by screening size-tunable homogenous embryoid bodies. Biomaterials *35*, 5987–5997.

Nakano, T., Kodama, H., and Honjo, T. (1994). Generation of lymphohematopoietic cells from embryonic stem cells in culture. Science *265*, 1098–1101.

Ng, E.S., Davis, R.P., Azzola, L., Stanley, E.G., and Elefanty, A.G. (2005). Forced aggregation of defined numbers of human embryonic stem cells into embryoid bodies fosters robust, reproducible hematopoietic differentiation. Blood *106*, 1601–1603.

Nurnberg, P., Thiele, H., Chandler, D., Hohne, W., Cunningham, M.L., Ritter, H., Leschik, G., Uhlmann, K., Mischung, C., Harrop, K., et al. (2001). Heterozygous mutations in ANKH, the human ortholog of the mouse progressive ankylosis gene, result in craniometaphyseal dysplasia. Nat. Genet. *28*, 37–41.

Ochiai-Shino, H., Kato, H., Sawada, T., Onodera, S., Saito, A., Takato, T., Shibahara, T., Muramatsu, T., and Azuma, T. (2014). A novel strategy for enrichment and isolation of osteoprogenitor cells from induced pluripotent stem cells based on surface marker combination. PLoS One *9*, e99534.

Panicker, L.M., Miller, D., Park, T.S., Patel, B., Azevedo, J.L., Awad, O., Masood, M.A., Veenstra, T.D., Goldin, E., Stubblefield, B.K., et al. (2012). Induced pluripotent stem cell model recapitulates pathologic hallmarks of Gaucher disease. Proc. Natl. Acad. Sci. USA *109*, 18054–18059.

Pick, M., Azzola, L., Mossman, A., Stanley, E.G., and Elefanty, A.G. (2007). Differentiation of human embryonic stem cells in serum-free medium reveals distinct roles for bone morphogenetic protein 4, vascular endothelial growth factor, stem cell factor, and fibroblast growth factor 2 in hematopoiesis. Stem Cells *25*, 2206–2214.

Ran, F.A., Hsu, P.D., Wright, J., Agarwala, V., Scott, D.A., and Zhang, F. (2013). Genome engineering using the CRISPR-Cas9 system. Nat. Protoc. *8*, 2281–2308.

Reichenberger, E., Tiziani, V., Watanabe, S., Park, L., Ueki, Y., Santanna, C., Baur, S.T., Shiang, R., Grange, D.K., Beighton, P., et al. (2001). Autosomal dominant craniometaphyseal dysplasia is caused by mutations in the transmembrane protein ANK. Am. J. Hum. Genet. *68*, 1321–1326.

Taylor, R.M., Kashima, T.G., Hemingway, F.K., Dongre, A., Knowles, H.J., and Athanasou, N.A. (2012). CD14- mononuclear stromal cells support (CD14+) monocyte-osteoclast differentiation in aneurysmal bone cyst. Lab Invest. *92*, 600–605.

Watanabe, K., Ueno, M., Kamiya, D., Nishiyama, A., Matsumura, M., Wataya, T., Takahashi, J.B., Nishikawa, S., Nishikawa, S., Muguruma, K., et al. (2007). A ROCK inhibitor permits survival of dissociated human embryonic stem cells. Nat. Biotechnol. *25*, 681–686.

Wolins, N.E., Quaynor, B.K., Skinner, J.R., Tzekov, A., Park, C., Choi, K., and Bickel, P.E. (2006). OP9 mouse stromal cells rapidly differentiate into adipocytes: characterization of a useful new model of adipogenesis. J. Lipid Res. *47*, 450–460.

Yamamoto, T., Kurihara, N., Yamaoka, K., Ozono, K., Okada, M., Yamamoto, K., Matsumoto, S., Michigami, T., Ono, J., and Okada, S. (1993). Bone marrow-derived osteoclast-like cells from a patient with craniometaphyseal dysplasia lack expression of osteoclast-reactive vacuolar proton pump. J. Clin. Invest. *91*, 362–367.

Yoshimi, K., Kunihiro, Y., Kaneko, T., Nagahora, H., Voigt, B., and Mashimo, T. (2016). ssODN-mediated knock-in with CRISPR-Cas for large genomic regions in zygotes. Nat. Commun. *7*, 10431.

Zandstra, P.W., Conneally, E., Piret, J.M., and Eaves, C.J. (1998). Ontogeny-associated changes in the cytokine responses of primitive human haemopoietic cells. Br. J. Haematol. *101*, 770–778.

Stem Cell Reports, Volume *9*

Supplemental Information

Craniometaphyseal Dysplasia Mutations in ANKH Negatively Affect Human Induced Pluripotent Stem Cell Differentiation into Osteoclasts

I-Ping Chen, Raj Luxmi, Jitendra Kanaujiya, Zhifang Hao, and Ernst J. Reichenberger

Supplemental Data

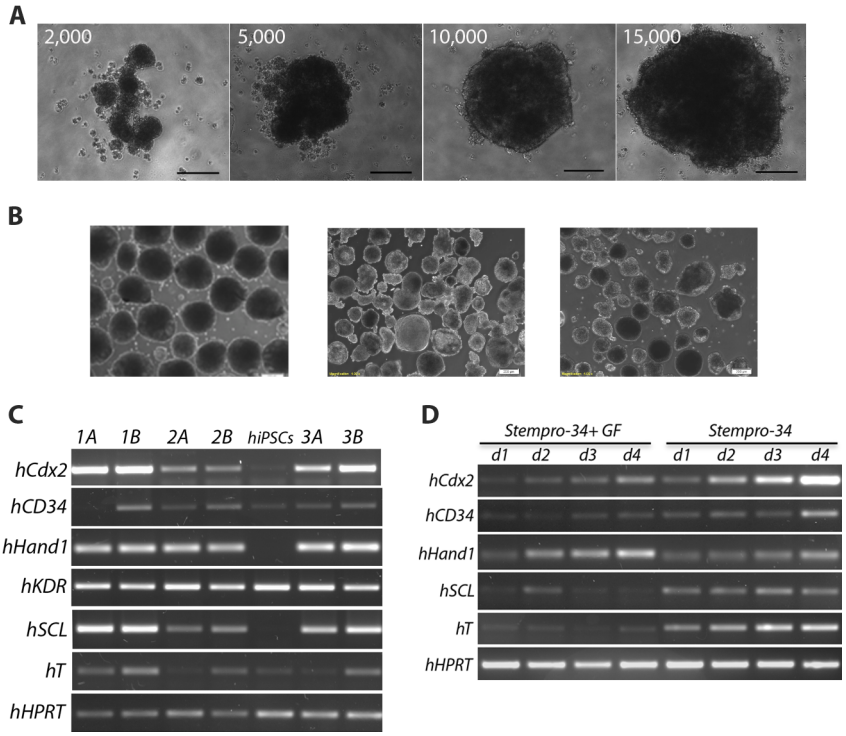

Figure S1. Promotion of mesoderm differentiation. Related to Figure 1 A) To generate relatively uniformly sized EBs, 2,000, 5,000, 10,000 and 15,000 cells/well were cultured on 96-well Nunclon Sphera microplates. Sizes of EBs are corresponding to the initial seeding densities. Scale bar=100µm. **B**) Sizes of EBs generated using our protocol (left panel, re-use the image of Figure 1B) are more homogenous compared to other published methods (middle and right panels) (1, 2). Scale bar=200µm. **C)** Optimization of culture conditions to promote EB mesoderm differentiation. Gene expression of mesoderm markers from day 4 EBs maintained under various culture conditions 1A, 1B, 2A, 2B, 3A and 3C (described in Table S1). **D**) Gene expression of mesoderm markers of EBs at day 1, 2, 3 and 4 cultured in Stempro-34 medium with or without supplementary growth factors (GF) provided with the Stempro kit. (n=3 technical replicates for each hiPSC line, 2 wild type hiPSCs used, 2 clones of each hiPSC line tested)

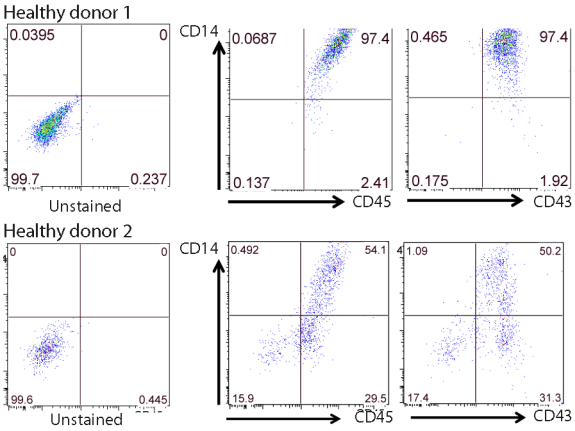

Figure S2. Related to Figure 1: Expansion analysis of myelomonocytic population collected at day 17 during Stage 2 from healthy donor 1 and 2 cultures. FACS analysis using cell surface markers CD14, CD43 and CD45. Negative staining controls are shown on left panel. (n=3 technical replicates for each hiPSC line)

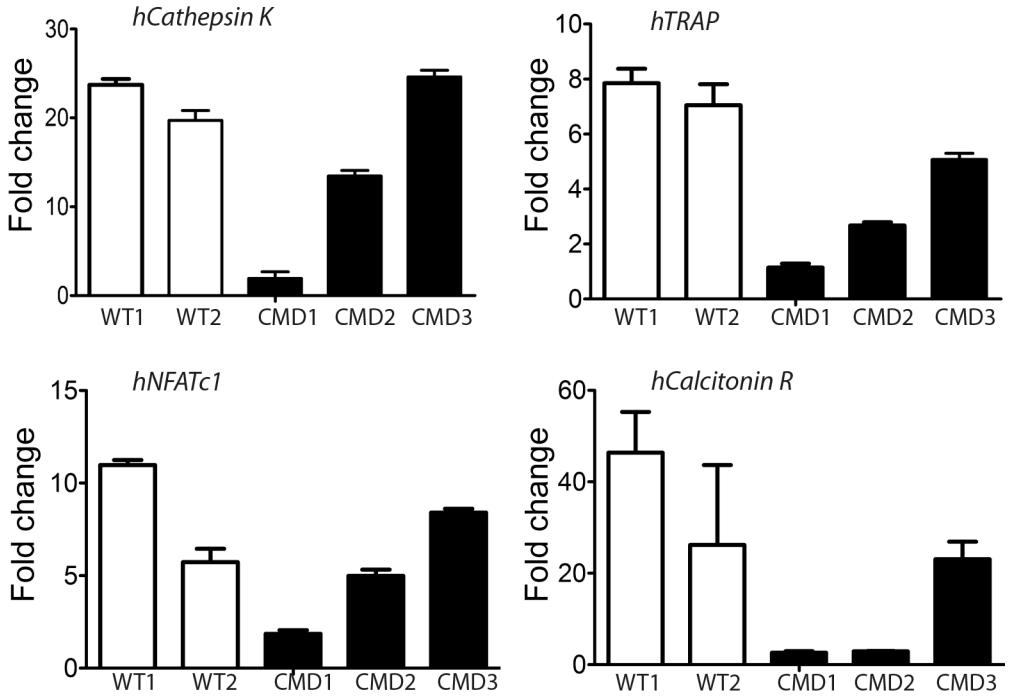

Figure S3. Related to Figure 2: Relative expression of osteoclast marker genes in individual hiPSC line from healthy donors and CMD patients shown by qPCR. Data presented are mean ± SD. (n=3 technical replicates for each hiPSC line)

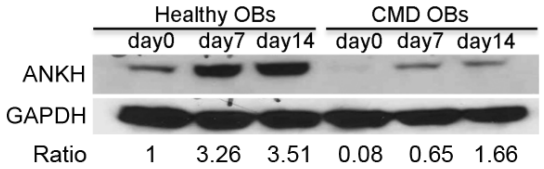

Figure S4. Related to Figure 3: A representative ANKH immunoblot of bone explant cultures from one healthy donor and one CMD patient differentiating for 0, 7, and 14 days. Numbers below indicate ratio of ANKH to GAPDH. (n=3 technical replicates)

Table S1: Culture conditions to maintain EBs derived from hiPSCs. Related to Figure 1.

Conditions	Culture medium	Cytokines
1A	Stempro-34, 2mM glutamine, 0.4mM MTG, A.A. 50µg/ml	Bmp4 (10) for 1 day, Bmp4 (10) + bFGF (5) for another 3 days
1 B	Stempro-34, 2mM glutamine, 0.4mM MTG, A.A. 50µg/ml	Bmp4 (25) + VEGF (50) for 2 days, day 2-4 Bmp4 (25), VEGF (50), SCF (50), TPO (50), FLT3 (50), bFGF (20)
2A	Stemline II, 20% FBS, 2mM glutamine, 0.4mM MTG, A.A. 50 µg/ml	Bmp4 (10) for 1 day, Bmp4 (10) + bFGF (5) for another 3 days
2B	Stemline II, 20% FBS, 2mM glutamine, 0.4mM MTG, A.A. 50 µg/ml	Bmp4 (25) + VEGF (50) for 2 days, day 2-4 Bmp4 (25), VEGF (50), SCF (50), TPO (50), FLT3 (50), bFGF (20)
3A	KO-DMEM, 20% FBS, 2mM L-glutamine, 0.1mM ME, 0.1mM NEAA	Bmp4 (10) for 1 day, Bmp4 (10) + bFGF (5) for another 3 days
3B	KO-DMEM, 20% FBS, 2mM L-glutamine, 0.1mM ME, 0.1mM NEAA	Bmp4 (25) + VEGF (50) for 2 days, day 2-4 Bmp4 (25), VEGF (50), SCF (50), TPO (50), FLT3 (50), bFGF (20)

MTG: monothioglycerol; A.A.: ascorbic acid; KO-DMEM: Knockout Dulbecco modificed Eagle medium; FBS: fetal bovine serum; NEAA: nonessential amino acids; ME: β-mercaptoethanol; cytokine concentrations in parentheses are ng/ml. Condition 1B was used in the described hiPSC osteoclast differentiation protocol.

Table S2: Primer sequences for qPCR. Related to Figure 2 and 3.

Gene	Forward primer	Reverse primer
CDX2	5'-CCCTAGGAAGCCAAGTGAAAACC-3'	5'-CTCCTTGGCTCTGCGGTTCTG-3'
CD34	5′-AAATCCTCTTCCTCTGAGGCTGGA-3′	5'-AAGAGGCAGCTGGTGATAAGGGTT-3'
Brachyury (T)	5′-TGTCCCAGGTGGCTTACAGATGAA-3′	5′-GGTGTGCCAAAGTTGCCAATACAC-3′
HAND1	5'-GAAAGCAAGCGGAAAAGGGAG-3'	5'-GGTGCGCCCTTTAATCCTCTT-3'
SCL	5'-AAGGGCACAGCATCTGTAGTCA-3'	5'-AAGTCTTCAGCAGAGGGTCACGTA-3'
CTSK	5'- CAGTGAAGAGGTGGTTCAGA -3'	5'-AGAGTCTTGGGGCTCTACCTT -3'
Calcitonin Receptor	5′-TCTCAGGAGTGAAAGCATTGCACATA -3′	5′-AATGCTATGACCGAATGCAGCAGTTA-3′
NFATc1	5'- AGAATTCGGCTTGCACAGG -3'	5'- CTCTGGTGGAGAAGCAGAGC -3'
TRAP (APC5)	5'-ACCTAGTTTGTTCTCTGATCGCCT-3'	5'-GGGATCTGTAATCTGACTCTGTCCTT-3'
HPRT	5'-ACTTGTCGCAGAAGCATC-3'	5'-GTGGGCGAACAGTGTAGAA-3'

Supplemental Experimental Procedures

Maintenance of human induced pluripotent stem cells (hiPSCs)

We maintained hiPSC cultures on plates coated with Matrigel (BD Biosciences) in PeproGrow hESC embryonic stem cell medium (Peprotech) which was changed every other day. Undifferentiated hiPSCs were passaged every 5 days by "cut and paste" technique.

Differentiation of hiPSCs into osteoclasts

We differentiated hiPSCs into mature and functional osteoclasts following a three-stage protocol. These steps were Stage 1) to induce mesoderm differentiation through EBs; Stage 2) to expand myelomonocytic populations released from attached EBs; Stage 3) to promote osteoclast maturation.

Mesoderm differentiation: For *in vitro* EB formation, day 5 undifferentiated hiPSCs were dissociated with Accutase cell detachment solution (EMD Millipore) for 10 minutes at 37°C. Single cells were washed in DMEM/F12 medium (Thermo Fisher Scientific) and centrifuged at 1300 rpm for 7 minutes. To induce mesoderm differentiation, EBs were generated by culturing 15,000 cells/well in 96-V Lipidure plates (NOF Corporation) or 96-U Nunclon plates (Thermo Fisher Scientific) in Stempro-34 (Thermo Fisher Scientific) medium and 5% PeproGrow hESC embryonic stem cell medium (Peprotech) supplemented with 2mM glutamine and $4x10^{-4}$ M monothioglycerol. Ascorbic acid (50 μg/ml), hBMP4 (25 ng/ml), hVEGF (50 ng/ml) and Rock inhibitor Y-27632 (10 μM) were freshly added into EB medium and cells were cultured in 5% CO_2 and 5% O_2. After culturing for 2 days, half of the medium was changed by adding Stempro-34 medium supplemented with ascorbic acid (50 μg/ml), hBMP4 (25 ng/ml), hVEGF (50 ng/ml), hTPO (50 ng/ml), hFLT3 (50 ng/ml), hSCF (50 ng/ml) and bFGF (20 ng/ml) for another 2 days in 5% CO_2 and 5% O_2. All cytokines were purchased from Peprotech Inc.

Myelomonocytic expansion: At day four, 40-50 EBs were transferred to one well of a 6-well plate coated with gelatin (EMD Millipore). To promote hematopoietic cell expansion, EBs were maintained in advanced DMEM medium (Thermo Fisher Scientific) supplemented with hIL-3 (25 ng/ml) and hMCSF (50 ng/ml) for 4 days in a cell culture incubator with 5% CO_2 and 5% O_2. Medium was changed every 4 days. hMCSF concentration was increased to 100 ng/ml after culturing EBs for 4 days and continued for another 13 days.

Osteoclast maturation: To generate mature and functional osteoclasts, single cells released from EBs attached on gelatin plate were collected and centrifuged at 1300 rpm for 7 minutes. Osteoclast progenitors were cultured in alpha MEM medium (Thermo Fisher Scientific) supplemented with 10% fetal bovine serum (Gibco), $2x10^{-7}$ M vitamin D (Sigma-Aldrich), hTGFβ (5 ng/ml), hMCSF (30 ng/ml) and hRANKL (50 ng/ml).

Human osteoblast explant cultures

Bone specimens were obtained after medically indicated surgery from one healthy donor and one CMD patient. Bone was cut into small pieces and maintained in DMEM (Gibco) until explant culture was confluent. Cells were then transferred to alpha-MEM (Gibco) osteoblast differentiating medium containing 10% fetal bovine serum (Gibco), 100 IU/ml penicillin, 100 μg/ml streptomycin (Gibco), 50 μg/ml ascorbic acid and 8 mM β-glycerophosphate (Sigma-Aldrich). The medium was changed every 2-3 days.

Flow cytometry analysis

To examine the progress of hematopoietic cell development, floating cells released from day 10, 13, 17 and 21 EBs (in Stage 2) were collected and stained with primary antibodies against CD14 (catalogue number 325604, FITC-conjugated, Biolegend), CD43 (catalogue number 560198, APC-conjugated, Miltenyi Biotec) and CD45 (catalogue number 304012, APC-conjugated, Biolegend) in 2% FBS/2mM EDTA/PBS. Cells were stained for 30 minutes in the dark and analyzed on a MACSQuant flow cytometer (Miltenyi Biotec). Samples without antibody staining were served as negative control.

RNA analysis

Total RNA from EBs and hiPSC-OCs was isolated using TRIzol (Thermo Fisher Scientific) followed by Direct-zol RNA extraction (Zymo Research) according to manufacturers' instructions. RNA was treated with DNase I (Invitrogen) and cDNA was synthesized by Superscript II reverse transcriptase (Invitrogen). qPCR was performed as described previously (3). Relative quantification of gene expression was

determined by the ΔΔCt method. Data was normalized to human *HPRT* gene expression. Primer sequences are listed in Supplemental Table 2.

Characterization of hiPSC-OCs

Osteoclast formation and bone resorption were examined by TRAP staining and bone resorption assays as described previously (3, 4). hiPSC OC precursors were plated on 12 mm glass slides in 24-well plates ($0.3x10^6$ cells per well) for TRAP staining and on bone chips ($0.1x10^6$ cells per bone chip) for bone resorption assays. Briefly, cells were washed twice with PBS, fixed with 2.5% glutaraldehyde and stained with TRACP (Lymphocyte Acid Phosphatase Kit; Sigma-Aldrich). TRAP images were taken by a Z1 Observer microscope (Zeiss). To analyze the resorption pits on bone chips, images from 6-8 bone chips were taken for each group and percent resorption was calculated as the ratio of resorbed area to total area using Image J software. To measure the size of osteoclasts, we chose the "region of interest" function in image J software to determine the osteoclast surface of more than 400 multinucleated ($n \geq 3$) TRAP positive cells per group. We selected the larger cells from three independent technical triplicates.

Generation of isogenic hiPSCs by CRISPR/Cas9 technology

We corrected the mutant allele (Ser375 deletion in *ANKH*) in hiPSCs from a CMD patient or created the mutant allele in hiPSCs from a healthy control individual by introducing a Phe377del mutation in *ANKH* using the CRISPR/Cas9 system. The CRISPR/Cas9 plasmid (Addgene) co-expressing a fused guide RNA/tracr RNA and Cas9 protein along with a targeting vector was electroporated into singularized hiPSCs. The tracr RNA recognized the guide RNA site and the Cas9 protein resulted in a targeted double strand break in the genome. The targeting vector was used to repair this double stranded break through the homology directed repair pathway. The targeting vector contained the desired genotype built into the homology arms along with a loxp-flanked selection cassette. After electroporation the cells were cultured and underwent antibiotic selection with G418. Once colonies appeared, they were picked and plated as isolated clones. These clones were genotyped by long-range PCR and sequencing for proper targeting and incorporation site of the desired allele. Silent mutations were introduced while correcting Ser375del mutation to minimize recutting a repaired site by subsequent nuclease binding. Positive clones were transfected with a plasmid transiently expressing CRE to remove the selection cassette.

Immunoblotting

Cells were lysed by RIPA lysis buffer (150 mM NaCl, 50 mM Tris, 1% NP40, 0.5% deoxycholate and 0.1% SDS) containing 1xHALT protease inhibitor cocktail (Thermo Fisher Scientific). The concentration of protein within the soluble protein lysate was determined by BCA protein assay (Thermo Fisher Scientific). The samples were run on SDS-PAGE gels and transferred onto PVDF membranes (BioRad) using a semi-dry transfer apparatus (Transblot; BioRad). The membranes were blocked in 5% skim milk Tris-buffered saline/Tween-20 (TBST) overnight and then probed with 1:1000 ANKH antibody (catalogue number AP9741b, Abgent) or 1:1000 ATP6v0d2 antibody (catalogue number sc-517031, Santa Cruz Biotechnology) in 1% skim milk TBST and subsequent goat anti-rabbit or anti-mouse horseradish peroxidase conjugated secondary antibody (Thermo Fisher Scientific). GAPDH antibody (catalogue number sc-25778, Santa Cruz Biotechnology) served as internal control. Protein bands were detected by enhanced chemiluminescent detection reagent (Azure Biosystems) and visualized by an Azure c600 imaging system (Azure Biosystems). Densitometric analyses of immunoblots were performed using Image J software.

Supplemental References

1. Cerdan C, Hong SH, and Bhatia M. Formation and hematopoietic differentiation of human embryoid bodies by suspension and hanging drop cultures. *Curr Protoc Stem Cell Biol.* 2007;Chapter 1(Unit 1D 2.
2. Grigoriadis AE, Kennedy M, Bozec A, Brunton F, Stenbeck G, Park IH, Wagner EF, and Keller GM. Directed differentiation of hematopoietic precursors and functional osteoclasts from human ES and iPS cells. *Blood.* 2010;115(14):2769-76.
3. Chen IP, Wang L, Jiang X, Aguila HL, and Reichenberger EJ. A Phe377del mutation in ANK leads to impaired osteoblastogenesis and osteoclastogenesis in a mouse model for craniometaphyseal dysplasia (CMD). *Human molecular genetics.* 2011;20(5):948-61.
4. Chen IP, Wang CJ, Strecker S, Koczon-Jaremko B, Boskey A, and Reichenberger EJ. Introduction of a Phe377del mutation in ANK creates a mouse model for craniometaphyseal dysplasia. *Journal of bone and mineral research : the official journal of the American Society for Bone and Mineral Research.* 2009;24(7):1206-15.